The *Arabidopsis* DREAM complex antagonizes WDR5A to modulate histone H3K4me2/3 deposition for a subset of genome repression

Yuqiu Wang[a,1], Yangyang Fan[a,1], De Fan[a,1], Yubo Zhang[b], Xiaoli Zhou[a], Ruikai Zhang[a], Yao Wang[c], Yujie Sun[c] ⓘ, Wei Zhang[d] ⓘ, Yuehui He[a] ⓘ, Xing Wang Deng[a,2] ⓘ, and Danmeng Zhu[a,2] ⓘ

The master transcriptional repressor DREAM (dimerization partner, RB-like, E2F and multivulval class B) complex regulates the cell cycle in eukaryotes, but much remains unknown about how it transmits repressive signals on chromatin to the primary transcriptional machinery (e.g., RNA polymerase II [Pol II]). Through a forward genetic screen, we identified BTE1 (barrier of transcription elongation 1), a plant-specific component of the DREAM complex. The subsequent characterization demonstrated that DREAM complex containing BTE1 antagonizes the activity of Complex Proteins Associated with Set1 (COMPASS)-like complex to repress H3K4me3 occupancy and inhibits Pol II elongation at DREAM target genes. We showed that BTE1 is recruited to chromatin at the promoter-proximal regions of target genes by E2F transcription factors. DREAM target genes exhibit characteristic enrichment of H2A.Z and H3K4me2 modification on chromatin. We further showed that BTE1 directly interacts with WDR5A, a core component of COMPASS-like complex, repressing WDR5A chromatin binding and the elongation of transcription on DREAM target genes. H3K4me3 is known to correlate with the Pol II transcription activation and promotes efficient elongation. Thus, our study illustrates a transcriptional repression mechanism by which the DREAM complex dampens H3K4me3 deposition at a set of genes through its interaction with WDR5A.

DREAM complex | transcriptional repression | H3K4 methylation

Transcriptional regulation is fundamental to all cellular events. RNA polymerase II (Pol II) initiates the transcription of protein-coding genes and some noncoding genes, and it undergoes subsequent pause/release, elongation, and termination steps (1). The conserved multiprotein machinery known as the DREAM complex (dimerization partner, RB-like, E2F and multivulval class B) represses gene expression and acts as the master player to regulate cell proliferation in eukaryotes (2, 3). However, little is known about how DREAM complex components communicate with the chromatin to alter Pol II activity and direct transcriptional repression.

The conserved multiprotein machinery known as the DREAM complex (dimerization partner, RB-like, E2F and multivulval class B) represses gene expression and acts as the master regulator of cell proliferation in eukaryotes (2, 3). Multivulval class B (MuvB) proteins were the first identified DREAM complex components in *Caenorhabditis elegans* (4, 5), and homologs were subsequently identified and characterized in *Drosophila melanogaster* (6, 7), mammals (8), and plants (9, 10). The MuvB core complex composed of LIN9, LIN37, LIN52, LIN54, and RBBP4 associates with E2F, DP, and RB-like proteins to form the multisubunit DREAM complex (2). Previous studies have shown that the nuclear-localized DREAM complex acts as the master regulator to maintain the quiescent state of the cell by binding to the chromatin of around a thousand cell-cycle genes and repressing their transcription in animals (2). In *Arabidopsis*, as core components of the DREAM complex, E2F transcription factors have been implicated in broad regulation of cell phase-specific gene expression, stem cell maintenance, and energy metabolism (11–14). Plant DREAM complex subunits have recently been systematically identified by immunoprecipitation-mass spectrometry and were shown to repress transcription of genes involved in cell-cycle control and DNA methylation maintenance (10).

Extensive studies have revealed that the histone modification H3K4me3 is actively associated with gene transcription in eukaryotes. In mammalian cells, the interaction of H3K4me3 with TAF3, a component of general transcription factor TFIID, is important for the preinitiation complex formation (15). In plants, H3K4me3 is linked to the transcription activation and promotes efficient transcription elongation (16, 17). H3K4me3 is catalyzed by the methyltransferases embedded in the conserved Complex Proteins

Significance

Transcriptional repressors such as the DREAM (dimerization partner, RB-like, E2F and multivulval class B)-related complexes are master regulators of the cell cycle, but much remains unknown about how binding of DREAM complexes controls gene expression. In this study, through a forward genetic screen we identified a plant-specific component of DREAM complex BTE1 (barrier of transcription elongation 1) in *Arabidopsis*. Our data showed that the interaction of BTE1 in the plant DREAM complex with Complex Proteins Associated with Set1 (COMPASS)-like complex component WDR5A contributes to the conserved DREAM complex-mediated transcription repression. H3K4me3 modification conferred by the COMPASS-like complex and methyltransferases in *Arabidopsis* is important for gene-specific RNA polymerase II (Pol II) transcription. We thus identified BTE1 as a key adaptor directly linking the promoter recognition and repression of Pol II elongation via the modulation of H3K4me3.

[1]Yuqiu Wang, Y.F., and D.F. contributed equally to this work.

[2]To whom correspondence may be addressed. Email: zhudanmeng@pku.edu.cn or deng@pku.edu.cn.

Associated with Set1 (COMPASS) or COMPASS-like complexes in yeast, mammals, and plants (18, 19). The COMPASS-like complex in *Arabidopsis* contains three structural components WDR5A, RbBP5 LIKE (RBL), and ASH2 RELATIVE (ASH2R) (19). There are two homologs of human WDR5, WDR5A, and WDR5B. The null mutant of *wdr5a* is lethal in both *Arabidopsis* and rice, while no obvious phenotypes of *wdr5b* mutants have been reported at present (20, 21). Previous studies have demonstrated that the interaction of multiple factors with WDR5A, including transcription factors, chromatin remodelers, and noncoding RNAs, could promote H3K4me3 deposition and activate the expression of genes involved in the regulation of flowering, grain yield, thermo-morphogenesis and endoplasmic reticulum stress (21–26).

In this work, by taking advantage of forward genetic screening, we performed comprehensive characterization of BTE1 (barrier of transcription elongation 1), a subunit of the plant DREAM complex (10) and revealed a transcription repression mechanism by which the DREAM complex specifically inhibits transcription of the noncoding RNA *HID1-LIKE 1* (*HIL1*) gene through its promoter binding in the tandem duplicated noncoding RNA gene pair, *HID1* and *HIL1*, within 2 kb in distance. More broadly, DREAM complex containing BTE1 generally represses hundreds of target genes by binding to their proximal promoters. We showed that BTE1 is recruited to chromatin of target genes by E2F transcription factors and that BTE1 inhibits WDR5A enrichment at target genes, resulting in a decrease in H3K4me3 and Pol II elongation, thus repressing transcription. Our study suggests that BTE1-WDR5A interaction appears to be a mechanism that contributes to DREAM complex-mediated transcription repression.

Results

Identification of *BTE1* as a Genetic Suppressor of *HID1*. For several years, we have studied the conserved noncoding RNA *HID1*, which engages in light-dependent biological processes and functions in transcriptional regulation (27, 28). By performing a sequence homology search, we identified *HID1-LIKE* 1 (*HIL1*) as a homolog of *HID1* (*SI Appendix*, Fig. S1), which sits 1.8 kb downstream of the *HID1* locus (Fig. 1*A*). In wild type (WT) seedlings, the expression level of *HID1* exceeds that of *HIL1* by more than five-fold (Fig. 1*A*). Under normal growth conditions, the 9-d-old seedlings of *hid1* mutants exhibited retarded and pointed leaf phenotypes (29) (Fig. 1*B* and *SI Appendix*, Fig. S2). Overexpression of *HIL1* in the single *hid1* mutant suppressed the *hid1* phenotype (Fig. 1 *B* and *C* and *SI Appendix*, Fig. S3*A*), suggesting the functional substitutability of *HID1* and *HIL1* during seedling development.

To further investigate why the expression of *HIL1* is controlled at a lower level compared to the expression of *HID1* in chromatin only as close as 1.8 kb, our study began with the attempt to identify genetic suppressor(s) of *HID1* through construction of an ethyl methane sulfonate (EMS) mutagenesis library of a *hid1 Agrobacterium* transferred DNA (T-DNA) insertion mutant. Screening of this library identified a total of five recessive suppressor mutants of *hid1*. All five mutants showed complete rescue of the *hid1* leaf phenotype to the WT phenotype at the seedling stage (Fig. 1*D* and *SI Appendix*, Fig. S3*B*). The mutation in each of the five mutants was found to map to one linkage group, which we named *BTE1* (barrier of transcription elongation 1) (Fig. 1*E*). We also showed that *hid1 bte1* double mutant seedlings phenocopied WT seedlings (Fig. 1*F* and *SI Appendix*, Fig. S3*C*). Cloning by resequencing confirmed that these five mutant

alleles represented mutations in a single gene: *AT2G40630* (*BTE1*). Further genetic analyses performed with FLAG- and (green fluorescent protein) GFP-tagged BTE1/*hid1 bte1* transgenic plants confirmed that *BTE1* functioned as a genetic suppressor of *HID1* (Fig. 1*F* and *SI Appendix*, Fig. S3*C*).

To examine the effect of the *BTE1* mutation in the *hid1* mutant, we first checked the expression of *HID1* and its homolog *HIL1*. Analysis of the *hid1 bte1* double mutant showed that *HIL1* expression was significantly increased in the double mutant in comparison with WT plants (Fig. 1*G*). In addition, further analysis of the *hid1 bte1-2 hil1* triple mutant, which was generated using CRISPR/Cas9 genome editing, indicated that the triple mutant phenocopied the single *hid1* mutant (Fig. 1 *H* and *I* and *SI Appendix*, Fig. S3*D*). These results suggest that, in WT plants, *BTE1* genetically acts through *HIL1* and represses its expression, while *HIL1* is highly expressed in *hid1 bte1* double mutants, in which it performs a function equivalent to that of *HID1*.

BTE1 Mediates Transcriptional Repression by the DREAM Complex. An early study in *Arabidopsis* reported that the WD40-repeat protein MSI1 (multicopy suppressor of IRA1) coprecipitates with BTE1 (30). A later study identified BTE1 as DREAM component 2 (DRC2) (10). To further characterize the function of *BTE1* within the DREAM complex, we examined the subcellular localization of BTE1. Experiments using plants expressing BTE1-GFP clearly indicated that BTE1 is mainly nuclear-localized (Fig. 2*A*). We further confirmed this conclusion via immunostaining assays using transgenic seedlings expressing BTE1-FLAG (Fig. 2*B*). Next, chromatin immunoprecipitation combined with high-throughput sequencing (ChIP-seq) analysis using a polyclonal BTE1 antibody generated in this study (*SI Appendix*, Fig. S4*A*) identified 1742 BTE1 peaks that were significantly enriched at the transcription start sites (TSS) of target genes, including *HIL1* (Fig. 2*C*). BTE1 occupies euchromatic loci of genes with moderate expression levels (*SI Appendix*, Fig. S4 *B* and *C*). Our BTE1 ChIP-seq and mRNA-seq analyses together revealed that the majority of differentially expressed and BTE1-bound genes showed up-regulated expression in the *bte1* mutant (116/118) (Fig. 2*D*). We defined a set of BTE1-unbound genes (control genes) with expression levels similar to those of the 116 BTE1 target genes in WT plants, and we found that the BTE1 target genes had significantly elevated expression levels in *bte1-2* plants in comparison with those of the control genes (Fig. 2*E*). These results indicate that BTE1 occupancy is negatively correlated with gene expression.

Pursuing the idea that BTE1 may mediate the transcriptional repression function of the DREAM complex, we monitored the impact of BTE1 on Pol II occupancy and global accumulation of nascent RNA. By performing Pol II ChIP-seq using an antibody that recognizes both phosphorylated and unphosphorylated forms of Pol II (total Pol II), as well as global nuclear run-on coupled deep-sequencing (GRO-seq) analyses, we found that the disruption of BTE1 function caused significant accumulation of Pol II and nascent RNAs on BTE1 target genes (Fig. 2 *F* and *G*), as illustrated by several examples (Fig. 2 *H* and *I*). These results suggest that BTE1 inhibits Pol II activity and represses target gene expression at the transcriptional level.

BTE1 is Recruited to Chromatin by E2F Transcription Factors. We next explored how BTE1 is deposited on chromatin by specifically focusing on three dominant suppressor mutations of *hid1* (1066A1, 475A2 and 199A1) identified in our aforementioned
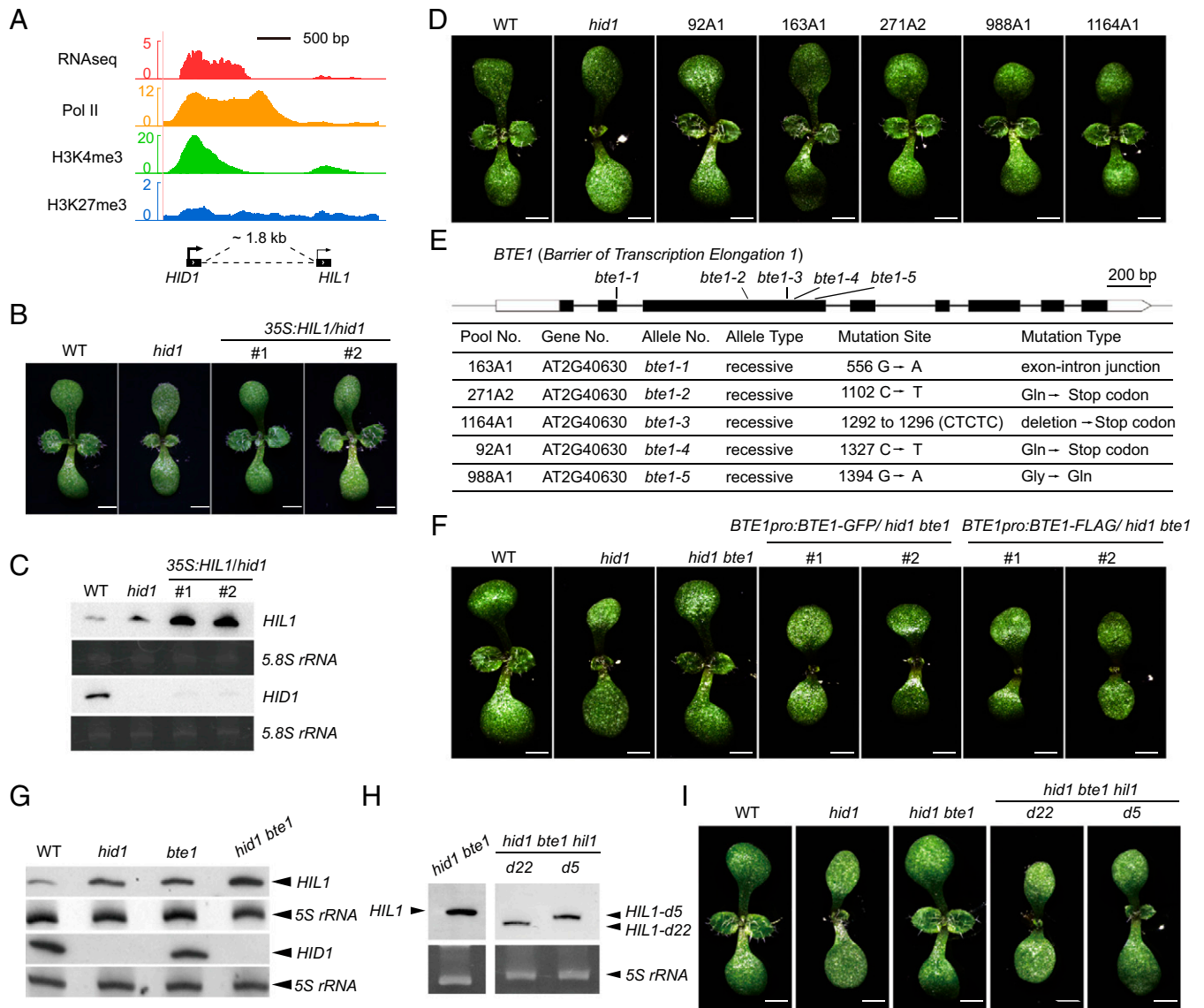
Fig. 1. *bte1* suppresses the retarded and pointed leaf phenotype of *hid1*. (*A*) Integrative genomics viewer (IGV) screen shots showing the RNA-seq and ChIP-seq signals of Pol II, H3K4me3, and H3K27me3 at the loci of *HID1* and *HIL1*. (*B*) Phenotypes of WT, *hid1*, and *35S:HIL1/hid1* transgenic seedlings. Scale bar, 1.5 mm. (*C*) Northern blots showing the expression levels of *HID1* and *HIL1* in WT, *hid1*, and the indicated transgenic lines, with *5.8S rRNA* as the loading control. (*D*) Phenotypes of WT, *hid1*, and five suppressor seedlings. Scale bar, 1.5 mm. (*E*) Schematic illustration of the *BTE1* gene model and a list of the mutation sites in each of the five suppressor lines. (*F*) Phenotypes of WT, *hid1*, *bte1hid1*, and the indicated transgenic seedlings. Scale bar, 1.5 mm. (*G*) Northern blots showing the expression levels of *HID1* and *HIL1* in seedlings of WT and the indicated mutants, with *5S rRNA* as the loading control. (*H*) Northern blots showing the expression levels of *HIL1* and its truncations in seedlings of *hid1 bte1* and *hid1 bte1 hil1*, with *5S rRNA* as the loading control. (*I*) Phenotypes of WT, *hid1*, *hid1 bte1*, and *hid1 bte1 hil1* seedlings. Scale bar, 1.5 mm.

genetic screen (Fig. 3*A* and *SI Appendix,* Fig. S5). Interestingly, these single nucleotide polymorphism (SNP) mutation sites were all positioned in the proximal-promoter region of *HIL1* (Fig. 3*B*), and analysis of seedlings harboring each of these sites revealed that *HIL1* expression was elevated to a high level similar to that observed in *hid1 bte1* mutants (271A2) (Fig. 3*C*); none of these suppressor mutations affected *HID1* expression. An mRNA-seq analysis of seedlings with the 475A2 allele revealed no obvious differences in global gene expression compared to WT seedlings (*SI Appendix,* Fig. S6). It was highly notable that these three suppressor mutations in the *HIL1* promoter region all map to a consensus cis-element that can be recognized by E2F transcription factor family members E2FA, E2FB, and E2FC (*SI Appendix,* Fig. S7). ChIP-qPCR analysis using BTE1 antibody showed that the BTE1 interaction with *HIL1* promoter region were significantly disturbed in *hid1hil1-2D* and *hid1hil1-3D* in comparison with WT (Fig. 3*D*). Reanalysis of our BTE1 ChIP-seq data using a peak

summit width of 200 bp showed that 36.2% (630/1742) of the BTE1-occupied genes had a consensus E2F-binding motif present at their BTE1 binding peak summit (*SI Appendix,* Fig. S7).

ChIP-seq using BTE1 and E2FA antibodies generated in this study and mRNA-seq analyses revealed that BTE1 and E2FA co-occupied 1,304 genes (Fig. 3*E* and *SI Appendix,* Fig. S8), of which 38 were up-regulated by at least 1.5-fold (false discovery rate < 0.05) in *bte1* mutant seedlings and seedlings of a weak *e2f* triple mutant (Fig. 3*F*). These results suggest that BTE1 and E2Fs work together to regulate transcription of these genes. We next assessed genome-wide chromatin occupation of BTE1 and E2FA and detected significant overlap between BTE1 and E2FA peaks at the TSS of target genes (Fig. 3*G*). After confirming that BTE1 interacts with E2F transcription factors in planta (*SI Appendix,* Fig. S9), we examined the interdependence of BTE1 and E2FA in chromatin binding. Combined analysis of our ChIP-seq data showed that although the levels of E2FA
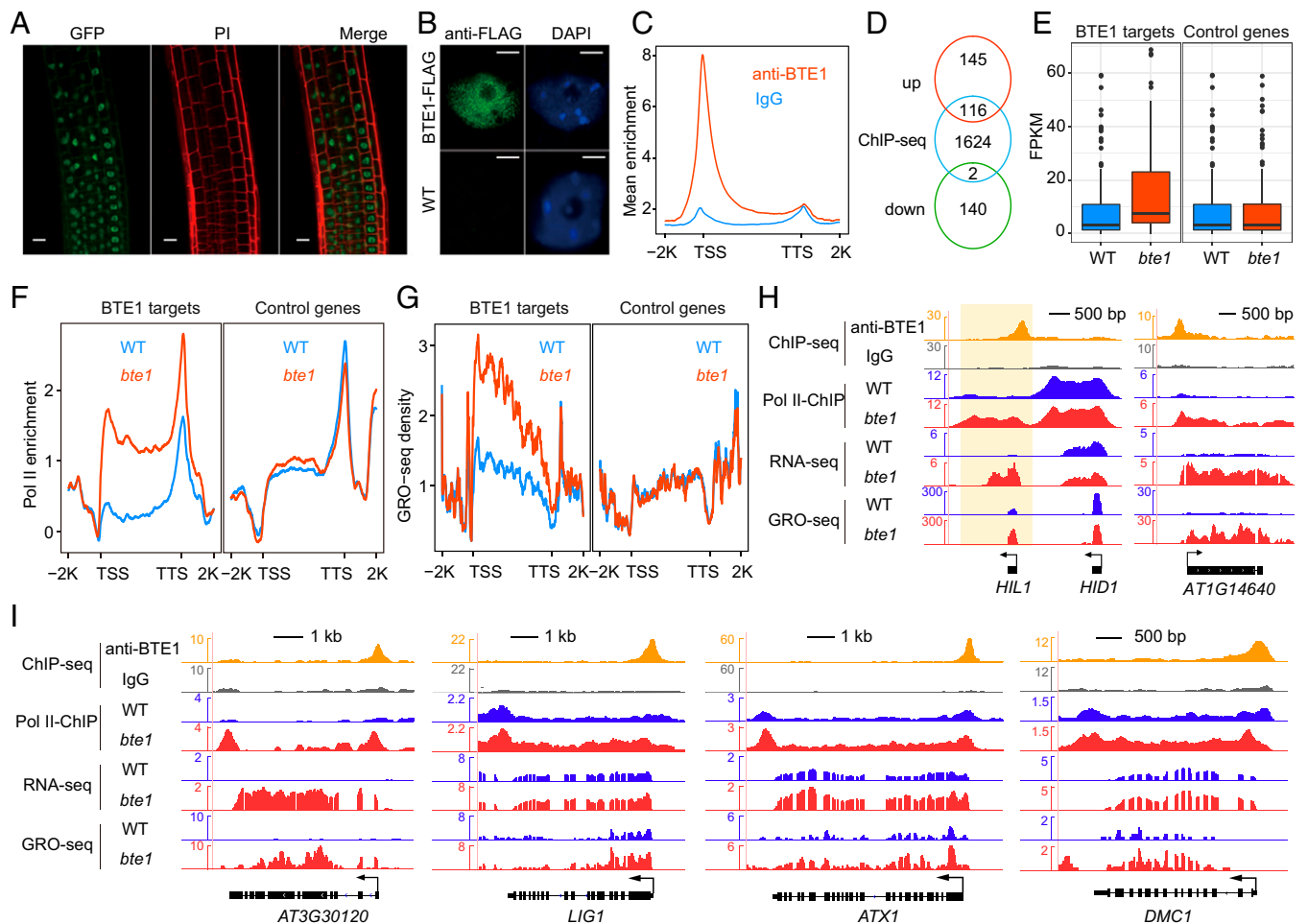
Fig. 2. BTE1 mediates transcriptional repression by the DREAM complex. (*A*) Confocal microscopy showing the nuclear localization of BTE1-GFP. Scale bar, 20 μm. (*B*) Immunofluorescence staining showing the nuclear localization of BTE1-FLAG. Scale bar, 5 μm. (*C*) Metaplot of the BTE1 ChIP-seq signal at target transcription units and flanking intergenic regions. The IgG ChIP-seq signal is shown as the negative control. (*D*) Venn diagrams displaying the statistically significant overlaps between genes differentially expressed in *bte1* and those bound by BTE1. (*E*) Box plots illustrating the expression levels of BTE1 target genes and control genes. FPKM, fragments per kilobase million. (*F*) Metaplot of RNA Pol II ChIP-seq. (*G*) Metagene analysis of the GRO-seq signal on the BTE1 target genes and control genes. (*H* and *I*) IGV screen shots showing signals of BTE1 ChIP-seq, IgG ChIP-seq, Pol II ChIP-seq, RNA-seq, and GRO-seq at individual BTE1 target genes. The gene models are shown at the bottom with black bars. The arrow indicates the direction of transcription.

binding to the TSS of its target genes were comparable in WT and *bte1* seedlings, the binding of BTE1 was dramatically decreased in the *e2f* triple mutants and *bte1-5* mutants, both globally (Fig. 3 *H* and *I*) and at individual loci (Fig. 3 *J* and *K*). Taken together, these results suggest that the dominant suppressor mutations impair the binding of BTE1 to the promoter of *HIL1* thus enhance *HIL1* expression, and clearly suggest that BTE1 is recruited by E2Fs to a subset of target genes, where it represses their transcription.

BTE1 Facilitates H3K4me2 and Inhibits H3K4me3 Deposition on its Target Genes. Seeking potential relationship(s) between distinct epigenetic states and BTE1-mediated gene repression of BTE1 target genes, we compared the epigenetic features of BTE1 target and control genes using a variety of publicly available histone modification profiling datasets (31). Intriguingly, we found that the density of three histone marks—H2A histone variant H2A.Z, H3K4me2, and H3K4me1—on BTE1 target genes was obviously higher than the corresponding density of each mark on the control genes (Fig. 4*A*), suggesting that these histone modifications are related to BTE1 binding. The H2A.Z ChIP-seq analysis revealed that the H2A.Z peaks downstream of the TSS in the WT plants showed stronger

enrichment at BTE1 target genes in comparison with control genes (Fig. 4 *B* and *F*). Additionally, the extent of H2A.Z incorporation around the TSS of BTE1 target genes in *bte1* seedlings was lower than that of WT seedlings. Along with the previously reported finding that *Caenorhabditis elegans* DREAM promotes H2A.Z incorporation on gene bodies to repress gene expression (32), our observations suggest that an increased extent of H2A.Z incorporation is also a feature of plant DREAM targets.

Interestingly, ChIP-seq analyses examining the effect(s) of BTE1 on the distribution of H3K4 methylation modifications showed that BTE1 facilitates H3K4me2 occupancy near the TSS of BTE1 target genes (Fig. 4 *C* and *F*). Given previous studies reporting that H3K4me2 modifications are not as strongly correlated with transcriptional activation as H3K4me3 (33–35), our results suggest that deposition of H3K4me2 is possibly linked with BTE1-mediated gene repression. Meanwhile, BTE1 represses H3K4me3 deposition around 5′-end of 83% (97/113) BTE1 target genes (Fig. 4 *D* and *F*). In addition, we found that BTE1 inhibits gene body deposition of H3K4me1 (Fig. 4*E*).

We next conducted MNase hypersensitivity sequencing (MH-seq) (36) to check the chromatin accessibility of DREAM
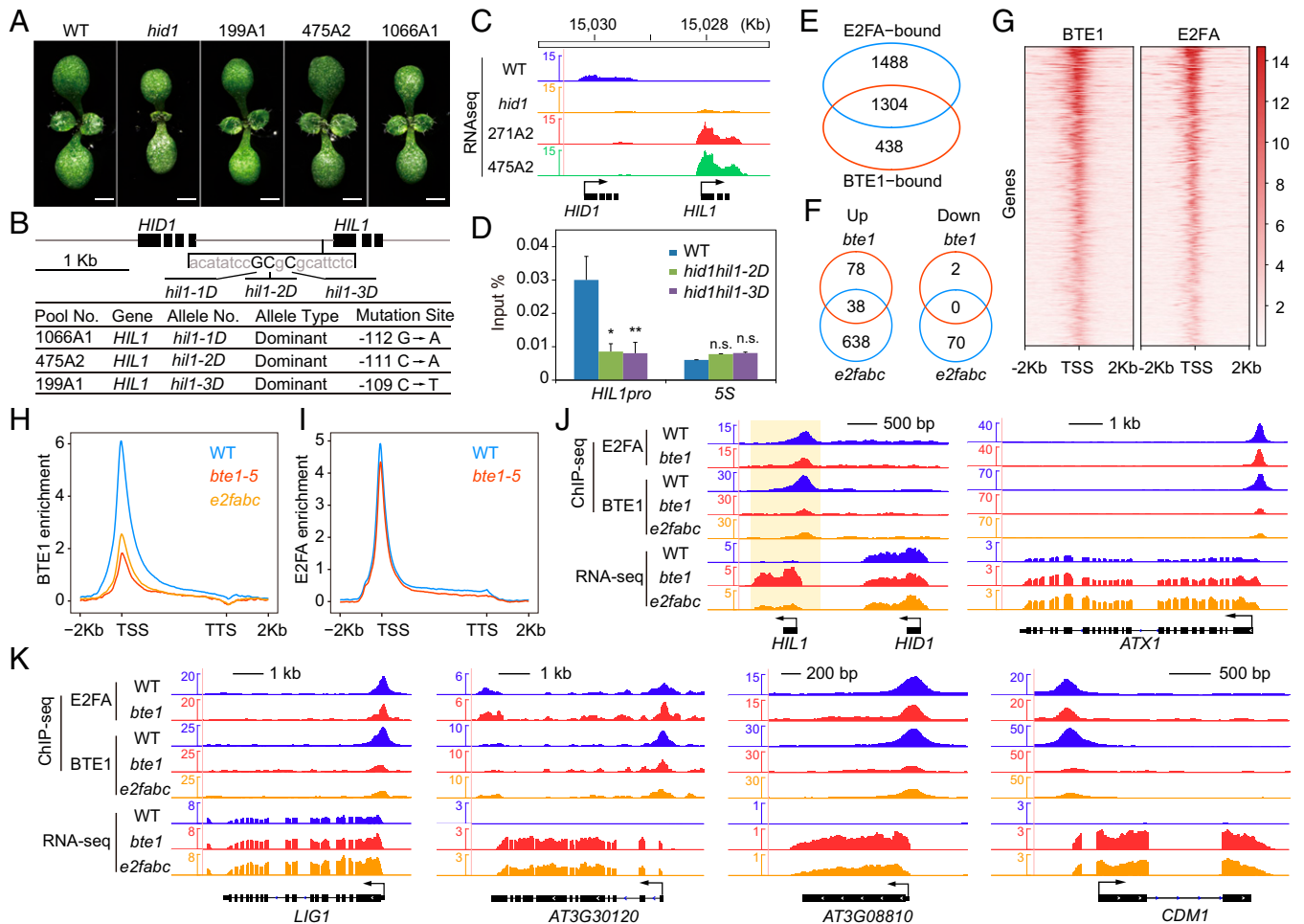
Fig. 3. BTE1 is recruited to chromatin by E2F transcription factors. (A) Phenotypes of seedlings of WT, *hid1*, and three dominant suppressor lines. Scale bar, 1.5 mm. (B) Schematic illustration of the gene locus of *HID1* and *HIL1*, and the mutation information identified in three *hil1* alleles. (C) Browser view of RNA-seq data in the genomic regions encompassing *HID1* and *HIL1*. The scale of normalized reads is shown. (D) ChIP-qPCR analysis of BTE1 interaction with the chromatin of *HIL1* promoter (*HIL1pro*). Data are presented as the mean ± SD (n = 3). *$P < 0.05$, **$P < 0.01$. n.s., no significance. (E) Venn diagram showing the overlap between BTE1-bound and E2FA-bound genes. (F) Venn diagrams showing overlaps between genes up-regulated (left) and down-regulated (right) in seedlings of *bte1* and *e2fa e2fb e2fc*. G, Heat-map of ChIP-seq signals of BTE1 (left) and E2FA (right) at their cobinding genes (n = 1,304). (H and I) Metagene profiles of ChIP-seq signals of BTE1 (H) and E2FA (I). (J and K) IGV screen shots of the E2FA ChIP-seq signal, BTE1 ChIP-seq signal and mRNA-seq datasets for representative BTE1 target genes as indicated. *e2fabc*: *e2fa e2fb e2fc* triple mutant. All tracks represent read density normalized to sequencing depth. The gene models are shown at the bottom as black bars. The arrow indicates the direction of transcription.

complex target genes using the seedlings of WT and *bte1* lines, which enabled us to precisely identify the open chromatin regions around the TSS of all genes. The chromatin accessibility of BTE1 target genes was obviously higher than that of the control genes, and this trend was moderately affected by *BTE1* depletion (*SI Appendix*, Fig. S10 *A* and *C*). Moreover, the repressive mark H3K27me3 was virtually undetectable at the BTE1 target loci in WT and *bte1* (*SI Appendix*, Fig. S10 *B* and *C*), suggesting that BTE1-mediated repression of transcription does not rely on this epigenetic mark. Thus, we speculate that the mechanism by which the DREAM complex represses gene expression is related to its inhibition of H3K4me3 deposition on the chromatin of its target genes.

BTE1 Interacts with WDR5A. We therefore performed yeast two-hybrid assays to identify BTE1-interacting protein(s) that could modulate H3K4me3. In the yeast two-hybrid assays, we detected interaction between BTE1 and WDR5A (Fig. 5*A*), a WD40-repeat protein homologous to a human protein that functions as a scaffold for histone-modifying complex assembly (20, 37). We further confirmed direct interaction between BTE1 and WDR5A using bimolecular fluorescence complementation (BiFC) and

coimmunoprecipitation (Co-IP) approaches (Fig. 5 *B* and *C*). In light of our finding that BTE1 does not modulate the expression or nuclear localization of WDR5A (*SI Appendix*, Fig. S11), we investigated the functional interaction(s) between these proteins. We next examined whether BTE1 affects the chromatin binding of WDR5A. To profile WDR5A occupancy on chromatin at a global level, we performed ChIP-seq assays using *WDR5A-HA* transgenic lines. In *bte1* plants, the occupancy of WDR5A-HA was dramatically increased at BTE1 target genes, but not at control genes (Fig. 5 *D* and *G*), suggesting that BTE1 can inhibit WDR5A chromatin binding. Since WDR5a was found to be a presenter for H3K4me3, the increase of H3K4me3 deposition in *bte1* appears to be resulted from the increased binding of WDR5a on the proximal promoter of BTE1 targets.

BTE1 Represses Pol II Elongation. Given that H3K4me3 at the 5′-end of actively transcribed genes promotes the productive elongation and that the elevated Pol II occupancy specifically observed at BTE1 target genes in *bte1* plants (Fig. 2*F*), it is plausible that BTE1 disrupts the chromatin binding capacity of Pol II. We therefore examined whether BTE1 disrupts Pol II initiation and/or elongation. In yeast and humans, the aforementioned
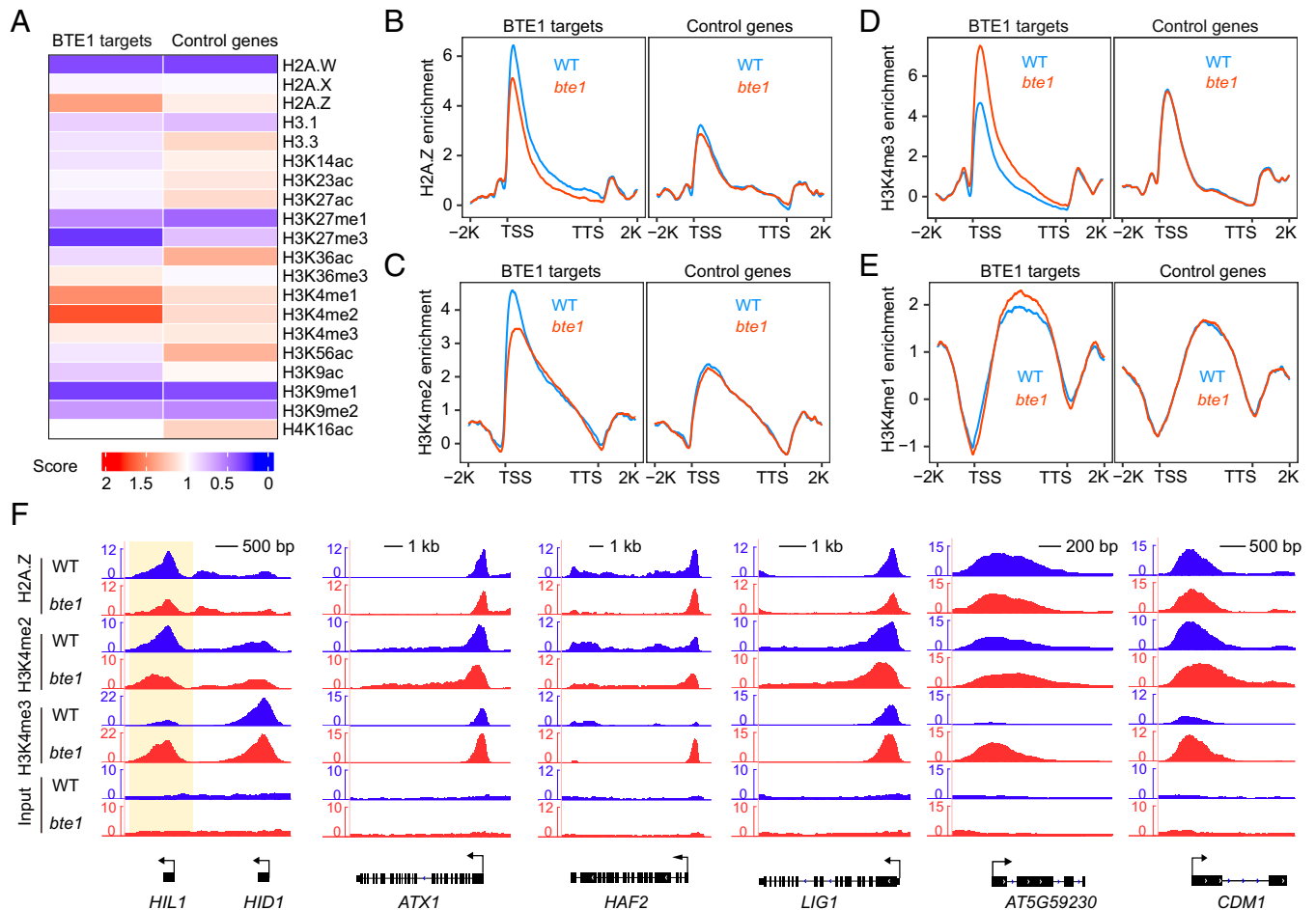
Fig. 4. BTE1 promotes H2A.Z and H3K4me2 deposition on its target genes. (*A*) Heat-map showing the enrichment (red) pattern of epigenetic features on BTE1 target genes and control genes compared with the average level of all genes. (*B–E*), Metaplots of ChIP-seq signals of H2A.Z (*B*), H3K4me2 (*C*), H3K4me3 (*D*), and H3K4me1 (*E*). (*F*) Integrative genomics viewer (IGV) screen shots showing the ChIP-seq signals of H2A.Z, H3K4me2, and H3K4me3 on the representative BTE1 target genes as indicated. All tracks represent read density normalized to sequencing depth. The arrow indicates the direction of transcription.

Ser5P and Ser2P modifications of Pol II are used as markers to experimentally distinguish Pol II initiation and elongation, respectively (38, 39). We conducted additional ChIP-seq analyses of *bte1* plants with antibodies against Ser5P and Ser2P. Consistent with previous reports (40, 41), we observed accumulation of Ser5P Pol II peaks around the TSS and TTS of BTE1 target genes in WT plants. A comparison against our matching data for WT plants showed that *bte1* mutants exhibited a slightly dispersed peak pattern for Ser5P Pol II occupancy at the TSS of BTE1 target genes, but a dramatic increase in Ser5P Pol II occupancy in the gene bodies of such genes (Fig. 5 *E* and *G*), suggesting that BTE1 also plays a role in Pol II elongation in comparison with its role in Pol II initiation. Consistently, analysis of the Ser2P Pol II dataset showed significantly increased Pol II occupancy of the gene bodies of BTE1 target genes in *bte1* plants in comparison with WT plants (Fig. 5 *F* and *G*). Together, these results show that BTE1-mediated repression of transcription of target genes results from its inhibition of H3K4me3 deposition and productive elongation by Pol II.

***BTE1* was Conserved in Plants and Duplicated After the β-WGD.** To further explore the biological function of *BTE1*, we compared the sequence of *BTE1* by BLAST in eukaryotic model organism species. Our BLAST searches indicated that *BTE1* is exclusive to the plant kingdom. Further genomic homology searches indicated that *Arabidopsis BTE1* and its homolog *BTE1-LIKE1* (*BTL1*), which share 32.48% sequence

similarity at the amino acid level, formed two distinct clades (Fig. 6*A*). Furthermore, our phylogenetic analysis indicated that *BTE1* is conserved in the land plants (*SI Appendix,* Fig. S12). Specifically, this bootstrap-supported analysis suggested a single origin of *BTE1* and *BTL1* in the Brassicales after the divergence of *Carica papaya* (Fig. 6*B* and *SI Appendix,* Fig. S13). Comparison of the findings from our analysis for the period after the *Carica papaya* divergence with previous evolutionary studies of angiosperms (42) clearly indicated that *BTE1* and *BTL1* represented a segment pair produced after the β whole genome duplication (β-WGD) (43, 44).

***BTE1* and *BTL1* Protect *Arabidopsis* Seedlings from Genotoxic Stress.** We next conducted mRNA-seq in *bte1* and *btl1* mutants and focused on up-regulated genes. The number of up-regulated genes (261) in the *bte1* mutant was greater than that of the *btl1* mutant (100) (Fig. 6*C*). The *bte1 btl1* double mutant exhibited more up-regulated genes (834) than either the *btl1* or *bte1* mutants (Fig. 6*C*). Gene Ontology (GO) analysis of the set of shared up-regulated genes for the *bte1* and *bte1 btl1* mutants indicated enrichment for terms related to DREAM complex target genes, including DNA replication, cell cycle, and DNA repair (Fig. 6*D*). Taken together, these results suggest that *BTE1* and *BTL1* have at least partially discrete functions in regulation of transcription. Consistently, similar, but not identical, GO terms were enriched among the set of up-regulated genes shared by the *btl1* and *bte1 btl1* mutants. It was also notable that the number
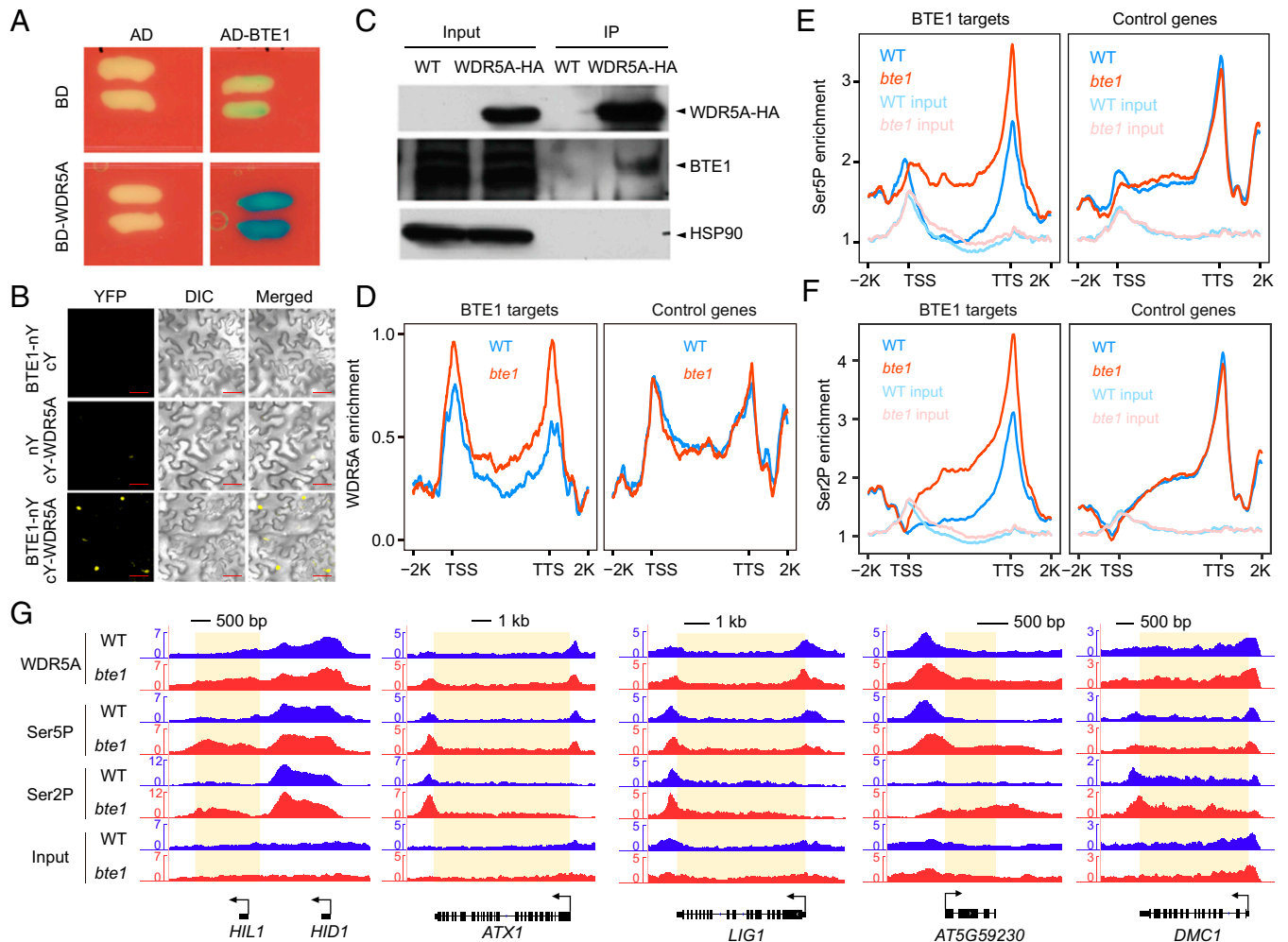
Fig. 5. BTE1 impedes the chromatin binding of WDR5A and represses Pol II elongation. (*A*) Yeast two-hybrid assay showing the direct interaction between BTE1 and WDR5A. BTE1 was fused with the activation domain (AD). WDR5A was fused with the DNA binding domain (BD). (*B*) BiFC assays for BTE1 and WDR5A interaction. nY: N-terminal of YFP; cY: C-terminal of YFP. Scale bar, 20 μm. (*C*) Co-IP assays showing the interaction between BTE1 and WDR5A. HSP90 was used as a loading control. (*D*) Metaplots based on the average enrichment of WDR5A occupancy for BTE1 target genes and control genes in WT and *bte1*. The *y* axis represents input-subtracted average ChIP-seq signal. (*E* and *F*) Metaplots of ChIP-seq signals of Ser5P-Pol II (*E*), and Ser2P-Pol II (*F*) for BTE1 target genes and control genes in WT and *bte1*. The input DNA-seq signal is displayed as the control in (*E*) and (*F*). (*G*) IGV screen shots of the ChIP signals of WDR5A-HA, Ser5P-Pol II, and Ser2P-Pol II for representative BTE1 target genes as indicated. The input track is displayed as the control. All tracks represent read density normalized to sequencing depth. The gene models are shown at the bottom as black bars. The arrow indicates the direction of transcription.

of genes associated with many of these DNA-related GO terms was consistently higher in the *bte1 btl1* mutants in comparison with either of the single mutants (Fig. 6*D* and *SI Appendix,* Fig. S14). These findings suggest that BTE1 and BTL1 may form two partially redundant DREAM complexes, while the DREAM complex containing BTE1 plays the predominant role in repressing gene expression. In a search for visible phenotypes of *bte1* and *btl1* mutants, we found that treatment of *bte1* (but not *btl1*) mutant seedlings with the DNA-damage-inducing agent bleomycin resulted in retarded leaf growth in comparison with that of WT plants. Bleomycin-treated *bte1 btl1* double mutant plants had a stronger leaf growth retardation phenotype than that of *bte1* plants (Fig. 6 *E* and *F* and *SI Appendix,* Fig. S15). These findings support the role of *BTE1* and *BTL1* in response to DNA damage.

Discussion

This study revealed how a plant-specific component in the DREAM complex mediates the transcription repression in *Arabidopsis*. Through the isolation and characterization of both

recessive and dominant suppressors of *hid1*, we provide strong genetic evidence demonstrating that the BTE1 subunit of the plant DREAM complex acts as a suppressor of *HID1* (Figs. 1 and 3). DREAM complex containing BTE1 directly binds to the promoter of *HIL1* to repress its expression. At the genome-wide level, DREAM complex containing BTE1 represses the transcription of more than 100 target genes, including genes involved in control of the cell cycle, DNA replication and repair, etc. Recruited by E2F transcription factors, the DREAM complex containing BTE1 acts as a barrier on open chromatin around the TSS of target genes, inhibiting the chromatin binding of WDR5A that promotes H3K4me3 deposition and the occupancy of phosphorylated Pol II complex on BTE1 target gene bodies, thus represses genes transcription. We found in this study that H3K4me2 is enriched in the 5′ regions of BTE1 target genes and associated with BTE1-mediated gene repression. While the deposition of H3K4me1 in gene bodies of BTE1 target genes is inhibited by BTE1 (Fig. 4). Although previous studies indicated that H3K4me1 is functional associated with transcription activation at specific loci (45, 46), at the global level H3K4me1 seems not to be associated with
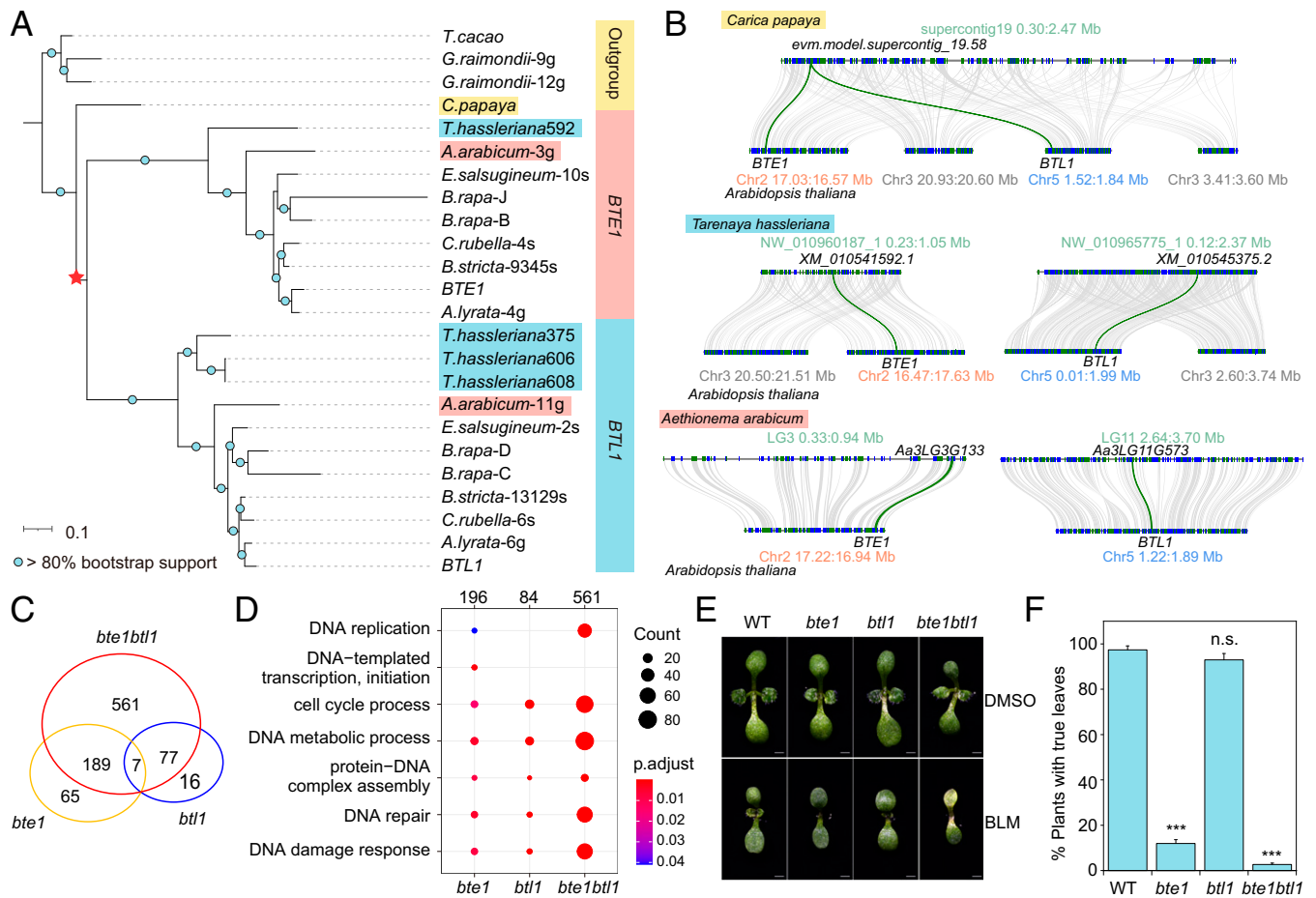
Fig. 6. *BTE1* was duplicated after the β whole genome duplication (β-WGD) and protects *Arabidopsis* seedlings from genotoxic stress. (*A*) A maximum likelihood-phylogeny for the homologs of *BTE1* and *BTL1* with the putative lineage. The β-WGD event is denoted with a red star. (*B*) Microsynteny analyses indicate the homologous regions between *Carica papaya* and *A. thaliana*, between *Tarenaya hassleriana* and *A. thaliana*, and between *Aethionema arabicum* and *A. thaliana*. (*C*) Venn diagrams showing overlaps among genes up-regulated in *bte1*, *btl1*, and *btel btl1* seedlings compared to WT seedlings. (*D*) GO analysis of the up-regulated genes shared by *bte1* and *bte1 btl1* seedlings, those shared by *btl1* and *bte1 btl1* seedlings, and those up-regulated only in *bte1 btl1* seedlings. (*E* and *F*) Phenotypes (*E*) and the ratio of plants with true leaves (*F*) for WT, *bte1*, *btl1*, and *bte1 btl1* seedlings grown on Murashige & Skoog (MS) medium supplemented with dimethyl sulfoxide (DMSO) or 0.6 mg/L bleomycin sulfate. Data are presented as the mean ± SD from three biological replicates. Statistical significance was determined using Student's *t* test. ***$P < 0.001$. n.s., no significance.

activation of transcription (34). How BTE1 regulates the deposition of H3K4me2 and H3K4me1 on its target genes remains currently unknown and deserves further investigation.

Promoter-proximal pausing, best-characterized in metazoans, has been shown to be prevalent in the transition from transcription initiation to productive elongation on tightly regulated genes. Factors such as negative elongation factor (NELF) and DRB sensitivity-inducible factor (DSIF), which physically associate with Pol II, have been shown to regulate promoter-proximal pausing. Plants lack homologs of NELFs, and they generally do not use the same promoter-proximal pausing mechanism as animals for gene regulation (41). Alternatively, it appears that plants have different regulatory systems similar to promoter-proximal pausing; for example, the transcriptional corepressor TOPLESS mediates the inhibition of mediator complex activity at the promoter-proximal region of target genes to maintain a paused transcriptional state (47, 48). The inhibition of WDR5A and Pol II elongation by the conserved transcriptional repressor DREAM complex may represent another form of promoter pausing. It will be of great interest to identify the developmental and/or environmental signals that release DREAM^BTE1-mediated gene repression for rapid activation of gene transcription in the near future.

BTE1 and its paralog *BTL1* originated after the β-WGD (Fig. 6), which occurred around 66 million years ago at the Cretaceous-Paleocene boundary, during an environmentally harsh transition. During this period, Earth underwent dramatic environmental stresses, including cooling, extended darkness, and changes in atmospheric composition (49, 50). Further analysis of the sub-functionalization and/or neo-functionalization of *BTE1* and *BTL1* in response to environmental stresses will provide insight regarding the retention of the *BTE1*/*BTL1* gene pair in the Brassicale lineage. This plant-specific evolutionary innovation could be exploited as an alternative route for developing therapeutic and biotechnological tools requiring transcriptional-repression.

Materials and Methods

Plant materials and growth conditions, phenotype analyses, suppressor screen and gene mapping, plasmid construction, and the generation of transgenic plants are described in *SI Appendix, Materials and Methods*. The detailed procedures of northern blot analysis, western blot analysis, confocal microscopy, immunofluorescence assay, ChIP assay and library preparation, RNA isolation and RNA-seq library preparation, GRO-seq, MH-seq, yeast two-hybrid assay, bimolecular fluorescence complementation assay, coimmunoprecipitation assay, phylogenetic analyses, and synteny mapping are provided in *SI Appendix, Materials and Methods*. The primers and probes used in this study are listed in *SI Appendix, Table S1*.

Author affiliations: ªState Key Laboratory of Protein and Plant Gene Research, School of Advanced Agricultural Sciences and School of Life Sciences, Peking-Tsinghua Center for Life Sciences, Peking University, Beijing 100871, China; ᵇState Key Laboratory of Protein and Plant Gene Research, Peking-Tsinghua Center for Life Sciences, Academy for Advanced Interdisciplinary Studies, Peking University, Beijing 100871, China; ᶜState Key Laboratory of Membrane Biology, Biomedical Pioneering Innovation Center (BIOPIC), School of Life Sciences, Peking University, Beijing 100871, China; and ᵈState Key Laboratory of Protein and Plant Gene Research, Peking-Tsinghua Center for Life Sciences, Academy for Advanced Interdisciplinary Studies, School of Life Sciences, Peking University, Beijing 100871, China

Author contributions: Yuqiu Wang, X.W.D., and D.Z. designed research; Yuqiu Wang, D.F., X.Z., R.Z., and Yao Wang performed research; Yuqiu Wang, Y.F., Y.Z., Y.S., W.Z., Y.H., X.W.D., and D.Z. analyzed data; and Yuqiu Wang, Y.F., X.W.D., and D.Z. wrote the paper.

1. P. Cramer, Organization and regulation of gene transcription. *Nature* **573**, 45–54 (2019).
2. S. Sadasivam, J. A. DeCaprio, The DREAM complex: Master coordinator of cell cycle-dependent gene expression. *Nat. Rev. Cancer* **13**, 585–595 (2013).
3. Z. Magyar, L. Bögre, M. Ito, DREAMs make plant cells to cycle or to become quiescent. *Curr. Opin. Plant Biol.* **34**, 100–106 (2016).
4. E. L. Ferguson, P. W. Sternberg, H. R. Horvitz, A genetic pathway for the specification of the vulval cell lineages of *Caenorhabditis elegans*. *Nature* **326**, 259–267 (1987).
5. M. M. Harrison, C. J. Ceol, X. Lu, H. R. Horvitz, Some *C. elegans* class B synthetic multivulva proteins encode a conserved LIN-35 Rb-containing complex distinct from a NuRD-like complex. *Proc. Natl. Acad. Sci. U.S.A.* **103**, 16782–16787 (2006).
6. P. W. Lewis *et al.*, Identification of a Drosophila Myb-E2F2/RBF transcriptional repressor complex. *Genes Dev.* **18**, 2929–2940 (2004).
7. M. Korenjak *et al.*, Native E2F/RBF complexes contain Myb-interacting proteins and repress transcription of developmentally controlled E2F target genes. *Cell* **119**, 181–193 (2004).
8. L. Litovchick *et al.*, Evolutionarily conserved multisubunit RBL2/p130 and E2F4 protein complex represses human cell cycle-dependent genes in quiescence. *Mol. Cell* **26**, 539–551 (2007).
9. K. Kobayashi *et al.*, Transcriptional repression by MYB3R proteins regulates plant organ growth. *EMBO J.* **34**, 1992–2007 (2015).
10. Y. Q. Ning *et al.*, DREAM complex suppresses DNA methylation maintenance genes and precludes DNA hypermethylation. *Nat. Plants* **6**, 942–956 (2020).
11. D. Inzé, L. De Veylder, Cell cycle regulation in plant development. *Annu. Rev. Genet.* **40**, 77–105 (2006).
12. M. Wildwater *et al.*, The RETINOBLASTOMA-RELATED gene regulates stem cell maintenance in *Arabidopsis* roots. *Cell* **123**, 1337–1349 (2005).
13. Y. Xiong *et al.*, Glucose-TOR signalling reprograms the transcriptome and activates meristems. *Nature* **496**, 181–186 (2013).
14. M. Taylor-Teeples *et al.*, An *Arabidopsis* gene regulatory network for secondary cell wall synthesis. *Nature* **517**, 571–575 (2015).
15. M. Vermeulen *et al.*, Selective anchoring of TFIID to nucleosomes by trimethylation of histone H3 lysine 4. *Cell* **131**, 58–69 (2007).
16. Y. Ding *et al.*, ATX1-generated H3K4me3 is required for efficient elongation of transcription, not initiation, at ATX1-regulated genes. *PLoS Genet.* **8**, e1003111 (2012).
17. M. Fromm, Z. Avramova, ATX1/AtCOMPASS and the H3K4me3 marks: How do they activate *Arabidopsis* genes? *Curr. Opin. Plant Biol.* **21**, 75–82 (2014).
18. A. Shilatifard, The COMPASS family of histone H3K4 methylases: Mechanisms of regulation in development and disease pathogenesis. *Annu. Rev. Biochem.* **81**, 65–95 (2012).
19. D. Jiang, N. C. Kong, X. Gu, Z. Li, Y. He, *Arabidopsis* COMPASS-like complexes mediate histone H3 lysine-4 trimethylation to control floral transition and plant development. *PLoS Genet.* **7**, e1001330 (2011).
20. D. Jiang, X. Gu, Y. He, Establishment of the winter-annual growth habit via FRIGIDA-mediated histone methylation at *FLOWERING LOCUS C* in *Arabidopsis*. *Plant Cell* **21**, 1733–1746 (2009).
21. P. Jiang *et al.*, The COMPASS-like complex promotes flowering and panicle branching in rice. *Plant Physiol.* **176**, 2761–2771 (2018).
22. Z. T. Song *et al.*, Transcription factor interaction with COMPASS-like complex regulates histone H3K4 trimethylation for specific gene expression in plants. *Proc. Natl. Acad. Sci. U.S.A.* **112**, 2900–2905 (2015).
23. Y. Wang *et al.*, Overexpressing lncRNA *LAIR* increases grain yield and regulates neighbouring gene cluster expression in rice. *Nat. Commun.* **9**, 3516 (2018).
24. X. Zhao *et al.*, Global identification of *Arabidopsis* lncRNAs reveals the regulation of *MAF4* by a natural antisense RNA. *Nat. Commun.* **9**, 5056 (2018).
25. A. S. Fiorucci *et al.*, *Arabidopsis* S2Lb links AtCOMPASS-like and SDG2 activity in H3K4me3 independently from histone H2B monoubiquitination. *Genome Biol.* **20**, 100 (2019).
26. M. Xue *et al.*, The INO80 chromatin remodeling complex promotes thermomorphogenesis by connecting H2A.Z eviction and active transcription in *Arabidopsis*. *Mol. Plant* **14**, 1799–1813 (2021).
27. Y. Wang *et al.*, *Arabidopsis* noncoding RNA mediates control of photomorphogenesis by red light. *Proc. Natl. Acad. Sci. U.S.A.* **111**, 10359–10364 (2014).
28. Y. Wang, J. Li, X. W. Deng, D. Zhu, *Arabidopsis* noncoding RNA modulates seedling greening during deetiolation. *Sci. China Life Sci.* **61**, 199–203 (2018).
29. Y. Wang *et al.*, Genomic features and regulatory roles of intermediate-sized non-coding RNAs in *Arabidopsis*. *Mol. Plant* **7**, 514–527 (2014).
30. M. Derkacheva *et al.*, *Arabidopsis* MSI1 connects LHP1 to PRC2 complexes. *EMBO J.* **32**, 2073–2085 (2013).
31. Y. Liu *et al.*, PCSD: A plant chromatin state database. *Nucleic Acids Res.* **46** (D1), D1157–D1167 (2018).
32. I. Latorre *et al.*, The DREAM complex promotes gene body H2A.Z for target repression. *Genes Dev.* **29**, 495–500 (2015).
33. X. Li *et al.*, High-resolution mapping of epigenetic modifications of the rice genome uncovers interplay between DNA methylation, histone methylation, and gene expression. *Plant Cell* **20**, 259–276 (2008).
34. X. Zhang, Y. V. Bernatavichute, S. Cokus, M. Pellegrini, S. E. Jacobsen, Genome-wide analysis of mono-, di- and trimethylation of histone H3 lysine 4 in *Arabidopsis thaliana*. *Genome Biol.* **10**, R62 (2009).
35. Y. Liu *et al.*, H3K4me2 functions as a repressive epigenetic mark in plants. *Epigenetics Chromatin* **12**, 40 (2019).
36. H. Zhao *et al.*, Genome-wide MNase hypersensitivity assay unveils distinct classes of open chromatin associated with H3K27me3 and DNA methylation in *Arabidopsis thaliana*. *Genome Biol.* **21**, 24 (2020).
37. H. Xue *et al.*, Structural basis of nucleosome recognition and modification by MLL methyltransferases. *Nature* **573**, 445–449 (2019).
38. M. Hajheidari, C. Koncz, D. Eick, Emerging roles for RNA polymerase II CTD in *Arabidopsis*. *Trends Plant Sci.* **18**, 633–643 (2013).
39. K. M. Harlen, L. S. Churchman, The code and beyond: Transcription regulation by the RNA polymerase II carboxy-terminal domain. *Nat. Rev. Mol. Cell Biol.* **18**, 263–273 (2017).
40. C. Liu *et al.*, *Arabidopsis* ARGONAUTE 1 binds chromatin to promote gene transcription in response to hormones and stresses. *Dev. Cell* **44**, 348–361.e7 (2018).
41. J. Zhu, M. Liu, X. Liu, Z. Dong, RNA polymerase II activity revealed by GRO-seq and pNET-seq in *Arabidopsis*. *Nat. Plants* **4**, 1112–1123 (2018).
42. J. E. Bowers, B. A. Chapman, J. Rong, A. H. Paterson, Unravelling angiosperm genome evolution by phylogenetic analysis of chromosomal duplication events. *Nature* **422**, 433–438 (2003).
43. R. Ming *et al.*, The draft genome of the transgenic tropical fruit tree papaya (*Carica papaya* Linnaeus). *Nature* **452**, 991–996 (2008).
44. P. P. Edger *et al.*, The butterfly plant arms-race escalated by gene and genome duplications. *Proc. Natl. Acad. Sci. U.S.A.* **112**, 8362–8366 (2015).
45. X. Fang *et al.*, The 3′ processing of antisense RNAs physically links to chromatin-based transcriptional control. *Proc. Natl. Acad. Sci. U.S.A.* **117**, 15316–15321 (2020).
46. S. Inagaki, M. Takahashi, K. Takashima, S. Oya, T. Kakutani, Chromatin-based mechanisms to coordinate convergent overlapping transcription. *Nat. Plants* **7**, 295–302 (2021).
47. A. R. Leydon *et al.*, Repression by the *Arabidopsis* TOPLESS corepressor requires association with the core mediator complex. *eLife* **10**, e66739 (2021).
48. N. Morffy, L. C. Strader, Plant promoter-proximal pausing? *Nat. Plants* **7**, 862–863 (2021).
49. P. Schulte *et al.*, The Chicxulub asteroid impact and mass extinction at the Cretaceous-Paleogene boundary. *Science* **327**, 1214–1218 (2010).
50. S. Wu, B. Han, Y. Jiao, Genetic contribution of Paleopolyploidy to adaptive evolution in angiosperms. *Mol. Plant* **13**, 59–71 (2020).
51. Y. Wang *et al.*, GSE181489. Gene Expression Omnibus. https://www.ncbi.nlm.nih.gov/geo/query/acc.cgi?acc=GSE181489. Deposited 4 August 2021.